

This document is downloaded from DR-NTU, Nanyang Technological University Library, Singapore.

Title	Three-dimensional deformation and strain induced by municipal pumping, part 1 : analysis of field data.
Author(s)	Burbey, Thomas J.; Warner, Sandy M.; Blewitt, Geoff.; Bell, John W.; Hill, Emma M.
Citation	Burbey, T. J., Warner, S. M., Blewitt, G., Bell, J. W., & Hill, E. M. (2006). Three-dimensional deformation and strain induced by municipal pumping, part 1: Amalysis of field data. <i>Journal of Hydrology</i> , 319, 123-142.
Date	2005
URL	http://hdl.handle.net/10220/8299
Rights	© 2005 Elsevier. This is the author created version of a work that has been peer reviewed and accepted for publication by <i>Journal of Hydrology</i> , Elsevier. It incorporates referee's comments but changes resulting from the publishing process, such as copyediting, structural formatting, may not be reflected in this document. The published version is available at: [DOI: http://dx.doi.org/10.1016/j.jhydrol.2005.06.028].

Three-dimensional deformation and strain induced by municipal pumping, part 1: Analysis of field data

Thomas J. Burbey^{a,*}, Sandy M. Warner^{b,1}, Geoff Blewitt^{c,2},
John W. Bell^{c,3}, Emma Hill^{b,4}

^a*Department of Geosciences Virginia Tech 4044 Derring Hall Blacksburg, VA 24061, USA*

^b*Olver Incorporated 1116 South Main St., Suite 100 Blacksburg, VA 24060, USA*

^c*Nevada Bureau of Mines and Geology University of Nevada, Reno Mail Stop 178 Reno, NV 89557, USA*

Abstract

A 62-day controlled aquifer test was performed at the site of a new municipal well that penetrates a thick sequence of compressible basin-fill deposits in Mesquite, Nevada. Observation data were acquired from a high precision Global Positioning System (GPS) network to accompany the water-level data from the pumped well and a nearby observation well. The purpose of the investigation was to quantify and characterize three-dimensional surface deformation and strain associated with cyclic pumping and to evaluate aquifer properties on the basis of these data. Results indicate that both horizontal (<8 mm total displacement with 0.2 mm precision) and vertical deformation (<12 mm total displacement with 2 mm precision) were measured within the first 22 days of pumping with a slowly migrating outward wave of compressional strain in spite of the fact that an 83-m brittle unsaturated zone resided over the dynamically active aquifer. The hydraulic head and strain data indicate that steady-state pumping conditions were likely reached after 35–40 days. Results also indicate that vertical mechanical rebound occurs after about 35 days even though the rate of pumping remains unchanged. Strain analyses indicate that this result is due to the changing shape in the pore structure of the pumped aquifer as an elongation occurs in the horizontal direction to more than accommodate a small compressional strain in the vertical direction. Uniaxial specific storage was estimated from time-subsidence data to be 2.8×10^{-6} /m. GPS-observed deformations reveal a mechanical and hydraulic anisotropy field that increases in rotation toward the northwest and in magnitude from west to east at the study site. This represents the first investigation where the magnitude and direction of the hydraulic conductivity tensor of the aquifer is estimated without using well data.

Keywords: Land subsidence; Global positioning system; Aquifer deformation; Pumping tests; Strain; Anisotropy

* Corresponding author. Tel.: +1 540 231 6696; fax: +1 540 231 3386.

E-mail addresses: tjburbey@vt.edu (T.J. Burbey), gblewitt@unr.edu (G. Blewitt), ehill@unr.edu (E. Hill).

¹ Tel.: +1 540 552 5548; fax: +1 540 552 5577.

² Tel.: +1 775 784 6691; fax: +1 775 784 1709.

³ Tel.: +1 775 784 1939; fax: +1 775 784 1709.

⁴ Tel.: +1 775 784 6691; fax: +1 775 784 1709.

1. Introduction

Field-based land subsidence research has dealt primarily with measuring or monitoring vertical deformation using a variety of techniques including first-order leveling (Bell, 1981; Bell and Price, 1991; Bell and et al., 2002), extensometers (Riley, 1969, 1984; Shuman and Anderson, 1988; Pope and Burbey, 2004), GPS networks (Ikehara and Phillips, 1994; Ikehara and others, 1997; Sneed and et al., 2001; Bell et al., 2002) and most recently interferometric synthetic aperture radar (InSAR) (Galloway and et al., 1998; Amelung and others, 1999; Hoffmann et al., 2001; Bell et al., 2002).

The measurement of horizontal deformation due to imposed stresses associated with pumping in unconsolidated aquifer systems has been limited largely because (1) the theory used in evaluating volume strains assumes that horizontal strain components imposed by pumping are negligible, and (2) measurement of such strains associated with pumping are difficult or costly to quantify. Yerkes and Castle (1969) were perhaps the first to measure widespread horizontal strain and deformation associated with fluid withdrawal and their measurements indicate that horizontal deformation at the land surface can be of the same magnitude as vertical compaction. About the same time, Wolff (1970) measured the total radial strain surrounding a pumping well in an unconfined aquifer and identified a zone of radial compression and an outer zone of radial extension around the pumping well. Still, in regions where vertical subsidence is a major societal problem, such as in the desert southwestern United States, the typically thick unsaturated zone above confined aquifer systems is believed to inhibit or at least limit the potential for horizontal displacements. Burbey (2001a, b) was the first to report incremental horizontal deformation measurements along a borehole in such a setting in Las Vegas Valley. The data from a borehole inclinometer indicates that the brittle unsaturated zone moves passively over the dynamic aquifer at much the same magnitude as the saturated zone. These data suggest that horizontal deformation may play a significant role in the development of earth fissures as previously suggested by Helm (1994a, b), who discussed the mechanics fissure development and pointed out the importance of horizontal displacements in their genesis.

The scarcity of studies designed specifically for the collection of horizontal strain and deformation data suggest that much is yet to be learned from such movements including the role of such strains in the genesis of earth fissures and the nature of active forces and their resulting strains in heavily pumped unconsolidated aquifer systems. Unfortunately, the data that exist are static in nature. In other words, no time series horizontal deformation data are available from the onset of pumping and for the duration of a long-term aquifer test without interference from other system stresses (other pumping wells).

The objective of this investigation was to collect and analyze horizontal and vertical surface deformations resulting from pumping of a new municipal well in thick highly compressible deposits overlain with a thick unsaturated zone. These analyses were then used to characterize the aquifer system from which pumping occurs for municipal use in Mesquite, Nevada. High precision surface deformations were measured using GPS techniques. It was concluded at the outset of this investigation that if horizontal deformation due to pumping could be measured at the land surface, an assessment of the role of horizontal strain affecting aquifer storage would be evaluated analytically using the aquifer-test and GPS data. The

results of this study can be used to better understand the dynamic nature of skeletal response due to pumping, which will lead to the development of better aquifer management practices, particularly for those aquifers susceptible to earth fissures.

2. Study area and experimental design

Selection of the proposed study site had to meet several criteria for proper deformation monitoring including limited interference from stresses caused by pumping from adjacent areas. The Mesquite, NV area (Fig. 1) in the desert southwestern United States was considered an ideal location because it is a growing retirement community, where demand for water resources continues to increase and has led to the need for new high-capacity municipal wells in previously unstressed locations. The field location occurs within a thick sequence of alluvial sediments at the site of a newly installed municipal well (WX31) that had not previously been pumped before this investigation. Hence, any pumping was expected to result in nonrecoverable deformation because the preconsolidation head surface was assumed to be near or at the current regional potentiometric level.

Additional important factors for selection of the site include the fact that regional recharge is low and limited to small amounts of winter precipitation that fall on the adjacent surrounding mountains and percolates into the adjoining alluvial fan or into the deep underlying carbonate rocks through fracture networks in the mountainous consolidated rock masses. Hence, recharge into the aquifer at the study site is considered negligible from the standpoint of its influence in aquifer testing. Perhaps the most favorable criterion is the existence of a thick sequence of unconsolidated sands, silts and clays contained in the Muddy Creek Formation (discussed further in Section 2.1) in which the pumping well is screened. Finally, the area is considered to be radially isotropic (though we judge this to be a relatively weak assumption). That is, no known faults or significant lithologic changes are located within 6 km of the pumping well).

2.1. Hydrogeologic description of mesquite, NV

The study area is located in the Mesquite basin, one of the deepest structural basins in the Basin and Range Province of the southwest United States (Fig. 1). The basin's depth ranges from 1600 to 4830 m (Johnson et al., 2002). The basin is bounded by the Tule Spring Hills to the north, East Mormon Mountains and Mormon Mesa to the west, the Beaver Dam Mountains to the northeast, and the Virgin Mountains to the southeast and south. The Piedmont structural basin that underlies the field site is characterized by a 3000-m thick bottom unit composed of Mesozoic to Cambrian aged sandstones and carbonate rocks containing east-northeast striking faults (Langenheim et al., 2000). Nearly 1800 m of highly compressible unconsolidated sediments of Tertiary age and younger comprise most of the basin fill. The Muddy Creek Formation represents the lowest and thickest of these units representing all but about 50 m of the uppermost unconsolidated deposits (Dixon and Katzer, 2002).

The topmost alluvial unit above the Muddy Creek represents weathered materials ranging from gravel to sand in size. The thickness of the alluvial sediments varies across the study

area from a few meters to about 25 m, but they are invariably cemented with calcium carbonate when they occur far above the water table making for a brittle caliche layer that overlies the unconsolidated deposits below. In lower lying areas where saturated, these shallow deposits have been the source of water for some residences, but the water quality tends to be poor (Johnson et al., 2002).

The main hydrogeologic unit of the region is the Muddy Creek Formation, which is used by the Virgin Valley Water District for municipal pumping at six sites including the study site well (WX31). The Muddy Creek unit behaves as a confined to semi-confined aquifer and has been found to have especially high transmissivities along faults north of the Virgin River. The study area sits within the Jachens graben and may be faulted and fractured at depth. Although no faults are evident at the surface in the vicinity of well WX31, east-west trending faults may occur in the subsurface within Tertiary and older deposits. Water from the underlying sandstones and carbonates may leak upward to provide recharge to the Muddy Creek aquifer; however, no direct evidence or measurements of such a process exists.

Data from the well log of municipal well WX31 (Fig. 2) indicate that the Muddy Creek unit has several facies extending upward from the base of the available log (615 m below land surface) to the top of the unit (24 m below land surface) and include silty clay with sand stringers, silty sand with clay interbeds, silty sand, silty sand with gravel, and thin clay units generally a few meters thick (M. Johnson, Virgin Valley Water District, written communication, 2003). The Muddy Creek sediments were deposited in a fluvial-lacustrine environment, where four cycles of lake formation and destruction (by the Virgin River) are recorded (Dixon and Katzer, 2002). The cycles of fine grained and coarse grained sediments created a series of aquifers containing discontinuous clay interbeds separated by continuous confining units. The connectivity and transmissivities of the aquifers in the Muddy Creek unit vary significantly based on location. No additional well logs exist for this portion of the Muddy Creek north of the Virgin River; hence, no evaluation of the areal extent of the individual units can be made.

The general direction of regional steady-state groundwater flow through the Muddy Creek aquifer at the study site is southeast to northwest (Fig. 1). Groundwater movement tends to follow the topographic and surface-water gradient of the basin from the alluvial fans toward the Virgin River, which flows westward near the study area and ultimately discharges to Lake Mead southwest of the study area.

2.2. Stratigraphy and aquifer test design

The Virgin Valley Water District completed installation of a new municipal well (WX31) in May, 2003 in an area that has had little history of production or monitoring. This new well was used for a controlled 62-day aquifer test beginning on May 28th. Fig. 1 shows the location of the pumping well that was used for the aquifer test in this investigation, which is situated on the lower part of the alluvial fan approximately 2.5 km south of the Virgin River near the town of Mesquite. Fig. 2 shows the well construction and associated stratigraphy. Well WX31 was constructed to a depth of 500 m, has a diameter of 0.508 m (20 inches), and is screened (i.e. open to the aquifer) for 237.7 m in the lowest portion of the borehole. The screened interval, however, is not continuous. Three solid-cased zones occur in intervals

containing high amounts of clay. The depth to water before well production was 83 m below the ground surface. The water level at the study site likely varies little from season to season. The Muddy Creek aquifer is bounded by the top clay unit from a depth of 24–83 m and the bottom clay (with sand stringers) unit from a depth of 481 m to at least 600 m. Above the well screen are four thin clay beds (2–3 m thick) separated by silty-sand units. The well is screened in a silty sand unit (with and without gravel clasts) and a silty sandy unit with interbedded clay stringers.

Hourly monitoring of the hydraulic head response due to pumping was limited to two well locations. One transducer was installed in an outer access port outside the main borehole (WX31) to minimize well losses associated with the proximity to the pump. A second transducer was installed in the WL VX well (Fig. 1) located 1480 m to the north–northwest of the pumping well. The depth of WL VX is only 48.8 m and is screened in the bottommost 12 m. The initial water level was 48.7 m below the land surface before production began in Well 31. The land surface at the two wells differs by almost 30 m and the hydraulic head in WL VX is 3 m lower than at WX31 assuming steady-state flow conditions and falls within the range of the regional potentiometric gradient shown in Fig. 1. While the heads in the two wells are similar, WL VX is most likely only screened in a unit representing the topmost portion of the aquifer represented in WX31 and is located above the screened interval of this pumping well. The portion of the aquifer screened in WL VX is likely separated from the portion of the aquifer screened in WX31 by several semi-confining beds, but the lateral continuity of these clay-dominated units is unknown.

Other Water District wells were in production at the same time as WX31. Table 1 has the production of each well in cubic meters for the months before, during and after the aquifer test and their relative location to WX31. In June, July, and August of 2003 the only wells in production outside the study area were Wells 33 and 27. The closest producing well is at a distance of approximately 4 km and the cones of depression and radii of influence around these wells do not intersect. WX31 is the only well on the south side of the Virgin River in production from June–August and Well 30 has no influence on the water levels of WX31. Nonetheless, horizontal deformation has been shown theoretically to occur well beyond distances where drawdown is small or non-existent (Burbey, 2002).

Water-level monitoring at the two sites occurred continuously from one week prior to pumping (May 21st) to more than 60 days after pumping (July 31st). At the commencement of pumping, the well was cycled with intervals of 8 h of pumping followed by 8 h of recovery (no pumping). This cycling was consistent for the duration of the aquifer test (62 days) and was required by the Water District because of limited storage availability and well conditioning. The pumping rate was fairly steady at $0.189 \text{ m}^3/\text{s}$.

2.3. Monitoring land deformation with GPS

Historically, spirit leveling was used to monitor benchmarks in favor of GPS because conventional leveling was more precise and accurate. Improvements in receivers, antennas, and data processing methodology have since the last decade allowed for millimeter-precision GPS surveys, suitable for geophysical investigations (Blewitt, 1993, 1998).

The basic process of using GPS to determine a precise and accurate unknown location is

similar to trilateration. The GPS receiver uses the distances to at least four known satellite locations to determine the position of the receiver. The satellite locations are encoded into the signal received by the GPS receiver. The receiver calculates the distance between the satellites and itself by taking the time of signal transmission (encoded in the signal), and the signal reception and multiplying it by the speed of light. The accuracy and precision of the GPS calculated position dependent on several factors: the accuracy of the satellite position, the errors in the receiver clock, the atmospheric delays of the signal, and the reflection and refraction of the signal off of objects near the GPS receiver, referred to as multipath (Blewitt, 1997).

The occurrence of stresses imposed on the aquifer due to pumping result in deformation of the porous media in three dimensions. The land movement on the surface likely represents a masked or subdued record of the aquifer matrix movement because of the thick unsaturated zone overlying the dynamic aquifer. In an isotropic aquifer the radial response due to pumping is symmetrical about the pumping well, both in regard to hydraulic heads and aquifer deformation.

When choosing locations for the GPS receivers and antennas, several factors were considered in addition to the assumption of radial symmetry including distance from the well, accessibility of the site, and the precision obtainable at each monitoring site (i.e. the site had to be located far from objects that might interfere with the antenna's ability to receive GPS signals from the satellites). In addition to selecting locations for the receivers, the duration of the GPS campaign needed to be decided based on receiver availability and well production schedule.

The assumption of radial symmetry allowed for a linear array of GPS stations and greater spatial density of aquifer deformation measurements. Seven of the stations were placed along a water line at distances of 150–2000 m from the pumping well (Fig. 1). The distance between stations was relatively small (spacing ranged from 100 to 500 m), which allowed for better precision in the relative positions of each, and higher spatial resolution of the surface strain field.

Ground displacement needed to be measured before, during, and after the pumping well was put into production. Phase One of the campaign was the period prior to well production from April 30 to May 6. Phase Two was the period beginning on May 7 and ending on May 29 during the initial production of the well, and Phase Three was the period after the drawdown in the well had reached a new dynamic equilibrium from May 30 to July 9. During Phase Three, the number of receivers was reduced because of equipment availability. Table 2 summarizes the equipment and duration of each phase.

In addition to carefully designing each site location and duration, the GPS antenna type was selected to optimize the precision of the campaign. Choke ring antennas were chosen because they are designed reduce multipath by filtering out indirect phase signals, such as signals that reflect off sources (i.e. objects) near to the antenna. The antenna is mounted onto a bolt attached to a stable benchmark, whether natural (i.e. bedrock) or engineered (i.e. cement, tripod, etc.). Four different benchmarks were used at the GPS site locations; all of them were engineered benchmarks.

Of the four different station set-ups, the final results indicated that most ideal mount for the GPS antenna was a 2-m diameter, 2.5 m deep cement vault located at access points along a

water line. These vaults proved to be well coupled to aquifer matrix as evidenced by their stability during the drawdown equilibrium phase of pumping. A bolt was drilled into each cement pad and marked with a measuring point. The choke ring antenna was mounted to the bolt and the antenna height for each station was measured relative to the measuring point.

To obtain data in the far field, an antenna was also placed at WL05 and WL09 (Fig. 1), two wells that are no longer in service and are approximately 2700 and 2000 m from WX31, respectively. To prevent vandalism, metal wire fences enclose these well sites, which have the drawback of creating signal multipath. A tripod was used to mount the antenna higher off the ground (than the bolted cement benchmarks), but the fence still caused multipath interference. The precision at these sites was not as good as the sites along the waterline. Also, the tripods were not as stable as the bolted antenna mounts, because the tripod may move slightly during high winds and extreme changes in temperature.

An antenna and receiver was also placed at the WLVX well site, where one of the pressure transducers was located. This site used a tripod for the antenna, but was not enclosed by a fence. However, the problems in precision created by the tripod instability still existed. The final antenna and receiver set-up was installed at the WX31 well house, which is 5 m west of the pumping well. This location was designed to be a permanent station that automatically uploads the raw GPS data onto a server. A pole attached to the side of the building acts as a mount for the antenna, keeping the antenna above the height of the roof. A receiver and computer inside the well house were used to automatically upload the GPS data onto a remote server.

The GPS station data were collected every 20 s at each site. The data were downloaded to a computer every three days and at the same time the batteries for the receivers were replaced. Once all the data were collected and the campaign was over, the data were processed using Trimble GPSurvey Software. As a check, data were also processed using GIPSY-OASIS II from the NASA Jet Propulsion Laboratory which produced almost identical results. Fig. 3 shows the horizontal deformation incurred at the land surface after 22 days of pumping at each vault relative to VT14(benchmark). Clearly pumping has induced a component of deformation toward the east including station WX31. The motion at station WX31 may or may not be indicative of horizontal displacement of the pumping well 5 m away. Cyclical pumping tends to result in sediment production during the initial pumping phase that can artificially enhance horizontal deformation in the vicinity of the well. Hence, it can not be assumed that the motion observed at station WX31 represents that of the pumping well. In assessing the motions at each of the vaults, those nearest the pumping well have experienced the greatest deformation. In addition, an unexpected component of deformation occurred toward the south at the pumping well and at each vault location whose southward magnitude also increased relative to the proximity to WX31. Further examination of these deformations will be discussed later.

3. Aquifer test results

Cyclic pumping has had a dramatic affect on water levels in the vicinity of the pumping well with a rapid drawdown of nearly 10 m during pumping followed by a nearly equal recovery immediately after the pump is turned off (Fig. 4). The net water-level decline after

removing the drawdown and recovery cycles associated with cyclic pumping suggests that the long-term drawdown asymptotically approached 8 m after 35–40 days of pumping. The net daily volume of pumping during the test was 9028 m³. The large volume pumped and small overall drawdown suggests that the aquifer is highly transmissive. The small decline was surprising considering the high degree of fine-grained deposits contained within the pumped aquifer, which led to concern whether the small head decline would produce sufficiently measurable displacement at the land surface. The drawdown pattern appears to be indicative of a fully confined to leaky aquifer system.

At the more distant WLX well, total observed drawdown was approximately 3 cm during the aquifer test (Fig. 5). The response time was also delayed and led to speculations that the declines may be indicative of natural seasonal variations in the water level or simply fluctuations in the hydraulic gradient. It should be noted, however, that the well is approximately one tenth the total depth of WX31 and screened above a seemingly laterally continuous confining unit. The small decline due to pumping is also masked by the daily fluctuations of nearly five cm associated with tidal effects and other natural phenomena occurring in the aquifer that are not related to pumping. In further evaluation of the water-level declines using numerical simulations (to be discussed in Part 2), the small delayed head decline is the result of a slow pressure response to pumping as the pumping stress travels through the clay layers that separate WLX monitoring well and the pumping well.

3.1. Calculation of transmissivity and storage from aquifer tests

Time-drawdown data from the observation well located 0.5 m from WX31 were used to estimate transmissivity and storage, although storage estimates this close to the pumping well are probably not too reliable. The Theis, Cooper-Jacob, and Hantush methods were all used to estimate the hydraulic characteristics of the highly transmissive Muddy Creek aquifer system. The Theis method was applied to drawdown and pumping data from individual cycles (labeled as ‘short’ in Table 3) as well as with the average daily drawdown and pumping rates over the course of the aquifer test (labeled as ‘long’ in Table 3). The Hantush method was used only with the long-term average drawdowns and pumping rates. The Cooper-Jacob straight-line method was used with drawdowns at the top and bottom of the drawdown cycles shown in Fig. 4.

Table 3 reports the estimated transmissivity and specific storage values obtained using these methods along with a published transmissivity value from Dixon and Katzer (2002) for the Muddy Creek Formation 4500 north of the study area. This well is screened over several units so the transmissivity value represents a composite value for all the water bearing units in the Muddy Creek. The Theis and Cooper Jacob methods assume that the aquifer is fully confined. The Hantush method assumes a leaky confined aquifer with no contribution of water from storage in the confining layer. Regardless of the method or what portion of the drawdown curve is used, the estimated transmissivities were all within a factor of three. The Hantush method produced the lowest values and is likely due to contribution from leakage of rapidly dewatering clay interbeds.

For many of the methods or approaches used, the storage values obtained do not appear to be very reliable. In fact, where the specific storage values are not provided, the estimates of

storage coefficient obtained using these methods are unrealistic. These unrealistic estimates are believed to be mostly due to the proximity of the observation well to the pumping well. Even if we assume the estimated storage coefficient is acceptable, the estimation of skeletal specific storage is also difficult because it requires explicitly knowing the total thickness of compressible sediments responsible for the measured subsidence at land surface. The rapid equilibration of hydraulic heads in the screened interval and the fact that WLVS experienced little hydraulic response due to pumping suggests that the compaction is likely coming from the region open to the screen, which includes clay stringers and thin confining units. The screened interval (including blank sections) is 237.7 m and represents the value used to estimate hydraulic conductivity in Table 3.

4. GPS data analysis results

The position of each receiver was estimated independently each day. Because the GPS orbits are designed to have the satellite geometry repeat over the same Earth-fixed location once a day, multipath can be effectively removed by averaging the position over a 24-h period. In spite of the small overall drawdown, the GPS signals, particularly in the horizontal direction, produced well-defined and precise results to about 0.2 mm precision.

All of the displacements measured are relative to the vault 14 (VT14) reference station which is located 2000 m west of the pumping well (Fig. 1). Vertical and horizontal motion are expected to be small at this distant site relative to the other vaults that are considerably closer to the pumping well. The measured displacements whose locations were identified initially using eastings and northings have been converted into a cylindrical coordinate system for convenience because of the assumption of radial symmetry around the pumping well. Hence, observed movement in the radial, tangential, and vertical directions refers to the cylindrical coordinate system. The horizontal component of deformation normal to the radial component will be discussed separately in the section titled 'Estimation of horizontal anisotropy from GPS measurements'.

Prior to the onset of pumping, the land surface appeared to be deforming slightly in a westward direction away from the well (Fig. 6a). VT01's position at 7 days prior to pumping (-7 days) was 2 mm east (-2 mm) of the position at time zero (0 days). By -4 days the vault was two mm west (+2 mm) of the position at time zero. All the vaults' displacements followed similar patterns before pumping began, but VT01, VT02 and VT03 had the largest magnitude displacement. Forces causing the pre-pumping displacement could be the result of horizontal seepage associated with the regional hydraulic gradient, tectonics, or strain resulting from municipal pumping from Well 30 located 5600 m south of WX31.

At the commencement of pumping all vaults displaced to the east (toward the well) as indicated by negative displacement values (Fig. 6a); vaults closer to the well appear to have displaced more than those further away from the well indicating radial extension with the three vaults closest to the well moving at about the same rate while the vaults farther from the well displacing less. If the displacement data are plotted as a function of distance (Fig. 6b), it becomes more evident that the zone of maximum displacement is migrating outward from the pumping well with time. This migration of maximum displacement supports the theory of horizontal granular deformation (Helm, 1994a, b). Helm maintains that the rate of

migration is a function of the hydraulic diffusivity (K/S_s) and the square root of time. The observed slow migration is evidence of a potentially small hydraulic diffusivity, or more specifically a large specific storage. The estimated hydraulic diffusivity at the field site suggests that the migration of the zone of maximum deformation should move outward more quickly than observed. The observed slow migration may be influenced greatly, however, by the eastward motion of the pumping well itself (away from the vaults), or perhaps of cyclic pumping. This phenomenon will be addressed in Part 2, which will deal with numerical modeling aspects of this investigation.

During the last phase of monitoring from days 22–62, there appears to be little radial displacement (Fig. 6a), which is most likely due to drawdown approaching a new equilibrium (steady state) as implied in 4. As heads approach steady state, the velocity of solids approaches zero and the radial deformation ceases (Helm, 1994a, b).

The vertical displacement signal contains more variability than the radial displacement signal because the GPS measurements are less precise and vulnerable to larger errors (Fig. 7a). Prior to the onset of pumping, the signal at all monitoring stations oscillated between ± 5 mm (Fig. 7a). At the start of pumping (0 days), the station closest to the pumping well appears to subside slightly more than the adjacent station further from the well. The maximum displacement at VT01 is approximately 7.5 mm. In spite of the variability in the measured record, a time-dependent trend is observed in which the magnitude and area of deformation increase as a function of time for the first 20 days of pumping. After about 35 days (when only three stations remain), a slight rebound occurs and may be as much as 2.5 mm after 60 days of pumping. This rebound coincides with the hydraulic equilibrium of the system but is best assessed with strain analysis, which is discussed in a forthcoming Section 4.1.

A conservative estimate on the precision of the daily GPS positions is given by the one-standard deviation daily repeatability of the estimates after day 26, during the phase of drawdown equilibrium. By this method, we estimate the relative horizontal precision to be 0.2 mm over the shortest inter-station distances of 0.4 km, increasing to 0.6 mm over the longest distances of 1.6 km. The relative vertical precision ranges 1.5–3.3 mm from the shortest to longest distances. The scaling of errors with distance indicates that decorrelation of atmospheric delay increasing station separation is a dominant component of the error budget.

When evaluating vertical deformation as a function of distance from the pumped well (Fig. 7b), the noise in the signal is removed through smoothing and the results indicate that for the current pumping scheme most of the vertical displacement occurs within the first 15 days of pumping. It does not appear that slow drainage of semi-confining units is occurring, which would be evidenced by continued compaction even if steady-state hydraulic head conditions were achieved.

4.1. Calculation of storage from GPS data

Storage estimates made from aquifer-test data of WX31 using only hydraulic head data adjacent to the pumping well may lead to potentially significant errors. Specific storage

values listed in Table 3 are likely to be up to several orders of magnitude too large. This may largely be due to the proximity of the observation well to the pumping well. Burbey (2003) developed a method, whereby time-subsidence data can be used to evaluate the storage of the aquifer system and the specific storage and hydraulic conductivity of the compressible deposits. Analogous to the Cooper-Jacob approach, the method uses the amount of compaction that occurs over one log cycle of time since the start of pumping and can be written as

$$S^* = \frac{5.46\Delta bT}{Q} \quad (1)$$

where Δb is the amount of measured vertical compaction (from a GPS locality) over one log cycle of time, Q is the average daily pumping rate, and T is transmissivity estimated from the Theis (long) method (Table 3). The storage term S^* refers to a uniaxial skeletal storage coefficient in which storage contributions from horizontal strains are considered negligible and the contribution of storage from water expansion is ignored. The early time data (first 20 days) produce trend lines of nearly constant estimated slope on semi-log graphs for the three GPS receiver locations nearest the pumping well. The transmissivity value must come from a long-term estimate because the compaction data used come from the long-term changes in surface elevation associated with pumping. The estimated uniaxial skeletal storage coefficient using this method is 3.6×10^{-4} and represents an average system value that includes the aquifer and any rapidly draining interbeds. Using the same estimate for aquifer thickness as previously reported (237.7 m) the estimated skeletal specific storage is $1.5 \times 10^{-6}/\text{m}$, which is comparable to estimated deposits of similar origin and lithology in Arizona (Hanson, 1989). Assuming an average porosity of 0.30, the specific storage contribution from water expansion ($S_{sw} = \rho_w g n \beta$) is $1.3 \times 10^{-6}/\text{m}$, making the total uniaxial specific storage $2.8 \times 10^{-6}/\text{m}$, which is comparable only to the specific storage estimate from the Theis (short) method using only one pumping cycle (Table 3). This may indicate that storage estimates obtained from traditional methods (using a long term average drawdown) under the influence of cyclic pumping may produce storage values that are artificially high by as much as two orders of magnitude.

5. Measured strain and its relation to storage and drawdown

The theory of three-dimensional consolidation (Biot, 1941, 1955) has been extended to applications of pumped aquifers composed of unconsolidated highly compressible deposits (Helm, 1987; Burbey and Helm, 1999; Burbey, 2001a, b, 2003). Theoretical work has suggested that horizontal deformation may contribute significantly to aquifer storage (Burbey, 2001a, b) or to the genesis of earth fissures in arid-zone environments (Helm, 1994a, b; Burbey, 2002). Yet no time-dependent three-dimensional field data set has been available to evaluate the significance of the general theory, particularly where thick unsaturated deposits have been thought to mask such observations. The investigation at Mesquite, NV was intended to evaluate whether strains would be observed and if they could be accurately measured under conditions of small head changes with a thick unsaturated zone that behaves passively over a dynamic aquifer system.

Because the screened interval of the pumping well occurs over 237.7 m, we can use cylindrical coordinates for describing the displacement and strain fields. The displacement vector \mathbf{u} is described as

$$\mathbf{u} = u_r \hat{\mathbf{e}}_r + u_\theta \hat{\mathbf{e}}_\theta + u_z \hat{\mathbf{e}}_z, \quad (2)$$

where u_r , u_θ , and u_z are the directional components of displacement in the radial, tangential, and vertical directions, respectively, $\hat{\mathbf{e}}_r$, $\hat{\mathbf{e}}_\theta$, and $\hat{\mathbf{e}}_z$ are the unit vectors in these same directions. The gradient operator in cylindrical coordinates is

$$\nabla = \frac{\partial}{\partial r} \hat{\mathbf{e}}_r + \frac{1}{r} \hat{\mathbf{e}}_\theta \frac{\partial}{\partial \theta} + \hat{\mathbf{e}}_z \frac{\partial}{\partial z}. \quad (3)$$

The rate of change of \mathbf{u} in the direction of the unit vectors (the directional derivatives) are defined as

$$\mathbf{D}_r = (\hat{\mathbf{e}}_r \cdot \nabla) \mathbf{u} = \frac{\partial u_r}{\partial r} \hat{\mathbf{e}}_r + \frac{\partial u_\theta}{\partial \theta} \hat{\mathbf{e}}_\theta + \frac{\partial u_z}{\partial z} \hat{\mathbf{e}}_z \quad (4a)$$

$$\begin{aligned} \mathbf{D}_\theta &= (\hat{\mathbf{e}}_\theta \cdot \nabla) \mathbf{u} \\ &= \left(\frac{1}{r} \frac{\partial u_r}{\partial \theta} - \frac{u_r}{r} \right) \hat{\mathbf{e}}_r + \left(\frac{1}{r} \frac{\partial u_\theta}{\partial \theta} + \frac{u_r}{r} \right) \hat{\mathbf{e}}_\theta + \frac{1}{r} \frac{\partial u_z}{\partial \theta} \hat{\mathbf{e}}_z \end{aligned} \quad (4b)$$

and

$$\mathbf{D}_z = (\hat{\mathbf{e}}_z \cdot \nabla) \mathbf{u} = \frac{\partial u_r}{\partial z} \hat{\mathbf{e}}_r + \frac{\partial u_\theta}{\partial z} \hat{\mathbf{e}}_\theta + \frac{\partial u_z}{\partial z} \hat{\mathbf{e}}_z. \quad (4c)$$

The strain components are represented as the directional derivatives Eqs. (4a)–(4c) in the direction of the unit vectors and are readily evaluated as

$$\varepsilon_{rr} = \hat{\mathbf{e}}_r \cdot \mathbf{D}_r = \frac{\partial u_r}{\partial r} \quad (5a)$$

$$\varepsilon_{\theta\theta} = \hat{\mathbf{e}}_\theta \cdot \mathbf{D}_\theta = \frac{1}{r} \frac{\partial u_\theta}{\partial \theta} + \frac{u_r}{r} \quad (5b)$$

$$\varepsilon_{zz} = \hat{\mathbf{e}}_z \cdot \mathbf{D}_z = \frac{\partial u_z}{\partial z} \quad (5c)$$

$$\begin{aligned} \varepsilon_{r\theta} &= \frac{1}{2} (\hat{\mathbf{e}}_r \cdot \mathbf{D}_\theta + \hat{\mathbf{e}}_\theta \cdot \mathbf{D}_r) \\ &= \frac{1}{2} \left(\frac{1}{r} \frac{\partial u_r}{\partial \theta} - \frac{u_\theta}{r} + \frac{\partial u_\theta}{\partial r} \right) \end{aligned} \quad (5d)$$

$$\varepsilon_{\theta z} = \frac{1}{2}(\hat{\mathbf{e}}_{\theta} \cdot \mathbf{D}_z + \hat{\mathbf{e}}_z \cdot \mathbf{D}_{\theta}) = \frac{1}{2} \left(\frac{\partial u_{\theta}}{\partial z} + \frac{1}{r} \frac{\partial u_z}{\partial \theta} \right) \quad (5e)$$

and

$$\varepsilon_{zr} = \frac{1}{2}(\hat{\mathbf{e}}_z \cdot \mathbf{D}_r + \hat{\mathbf{e}}_r \cdot \mathbf{D}_z) = \frac{1}{2} \left(\frac{\partial u_z}{\partial r} + \frac{\partial u_r}{\partial z} \right). \quad (5f)$$

From these expressions, the normal components of strain can be summed to calculate the volume strain as

$$\varepsilon = \varepsilon_{rr} + \varepsilon_{\theta\theta} + \varepsilon_{zz} \quad (6a)$$

or

$$\varepsilon = \frac{\partial u_r}{\partial r} + \frac{u_r}{r} + \frac{\partial u_z}{\partial z}. \quad (6b)$$

Under uniaxial or vertical strain conditions as is traditionally assumed in ground-water flow systems in which compaction is measured, radial and hoop strain are zero and the vertical strain is assumed equal to the volume strain.

Measured GPS displacements at each station at the field site were converted to strain components assuming radial symmetry about the pumping well. Radial strain was calculated using successive station locations as

$$\varepsilon_{rr\frac{(i+1)+i}{2}} = \sum_{i=1}^N \frac{(U_{i+1} + U_i)}{1000(r_{i+1} + r_i)} \quad (7)$$

where U_{i+1} is the measured radial component of displacement at a more distant vault from the pumping well, U_i is the measured radial component of displacement at the next nearest vault to the pumping well, and r is the radial distance from the respective vaults to WX31 (the conversion factor of 1000 is required for consistent units), and N is the total number of vaults. The calculated value was assumed to be at a radial distance half way between two successive stations. Fig. 8 shows the complex nature of the radial strain component as a function time for several of the vault locations. Near the pumping well ($r=205$ m) radial strain is compressive, while at $r=660$ m extensional strain reaches a maximum during much of the time after the start of pumping. At greater distances the extensional strain is less. This complex behavior of radial strain can be best described using Fig. 6b. The slope of the radial displacement plots shown in Fig. 6b (as a function of distance) represent the radial strain and the zone of compressive strain is actually migrating slowly outward with time even as the magnitude of total displacement increases at all locations. The peak displacement at any point in time represents a point (or more likely a zone) of zero radial strain. The apparent eastward migration of the pumping well or the pulsed pumping associated with well WX31 is a likely factor in the slow migration of the zone of zero radial strain because the pumping rate is zero for about half of the time during the duration of the aquifer test.

Hoop strain represents the tangential strain occurring as a result of radially converging particle path lines toward the pumping well. In an analogous fashion to the radial strain, the

normal component of tangential strain can also be calculated as

$$\varepsilon_{\theta\theta_{((i+1)+i)/2}} = \frac{(U_{i+1} + U_i)/2}{1000(r_{i+1} + r_i)/2} \quad (8)$$

where U is the measured displacement at vault i . The mean displacement between successive vaults is used to assure that the strain component is measured at the same midpoint location as Eq. (6a and 6b). Fig. 9 reveals that after the start of pumping, hoop strain is compressive for all radial distances from the pumping well and can, theoretically, represent the largest component of strain and ultimately storage released to the well (Burbey, 2001a, b). After 22, days the magnitude of hoop strain approaches a constant value at each radial distance as the aquifer system approaches hydraulic equilibrium.

Areal strain, ε_A , represents the sum of the radial and hoop strain components and is useful for comparing the total horizontal strain to the vertical strain. Areal strain can be computed as follows

$$\varepsilon_{A_{(i+1)+i}} = \frac{\pi[(r_{i+1} + U_{i+1})^2 - r_{i+1}^2] - [(r_i + U_i)^2 - r_i^2]}{\pi[r_{i+1}^2 - r_i^2]} \quad (9)$$

where the displacements and radial distances are expressed in common units. Finally, the volume strain represents the sum of the areal strain and the vertical strain components and is expressed in Fig. 10. This illustration clearly shows that near the pumping well a large component of the total strain, and therefore storage, originates from horizontal strain components. This indicates that one-dimensional subsidence models would tend to over-predict compaction or storage near the pumping well.

The calculated vertical strain signal (Fig. 11), like vertical displacement, has a significant amount of noise, making it difficult to distinguish the real signal. The vertical strain is estimated using Eq. (5c) by dividing the mean daily measured vertical displacement difference between the elevation of the land surface prior to pumping with the measured value at a particular time at each vault and dividing by the distance over which vertical displacement is assumed to occur. This vertical distance is estimated from the lithologic log and water-level information to be approximately 350 m, a thickness that is slightly greater than the difference of the top to the bottom elevations of the well screen.

In all of the strain diagrams (Figs. 8–11), strain was occurring prior to the start of pumping (-7–0 days); however no consistent trend was observed. These initial strains could be caused by (1) settling of the GPS equipment in the field as it adjusted to the temperatures and mountings, (2) a pump test conducted by the Virgin Valley Water District for several hours two days before the start of the aquifer test, (3) other more distant municipal pumping wells used by the Water District, (4) regional tectonic movement or (5) horizontal seepage forces due to the natural hydraulic gradient. The source of the strain is difficult to delineate because of the variation in the strain magnitudes.

To evaluate the contribution of each strain component to the total volume strain caused by pumping, the strain components were plotted on a single graph (Fig. 12). This figure clearly

shows that near the pumping well the contribution of hoop strain exceeds the vertical strain; whereas the radial strain only contributes marginally to the total water produced except within about 300 m from the pumping well. It should be noted that theoretically both hoop strain and radial strain are zero at the pumping well provided the well is fixed. At the Mesquite site these horizontal strain components are nonzero at station WX31 (5 m from pumping well) and are greatest between station WX31 and the first vault at a radial distance of 140 m. The radial strain component is largely extensional (>0) with increasing distance from the pumping well and indicates that in the radial direction porosity is increasing, whereas in the vertical direction porosity is decreasing. Therefore the shape of the pore structure is being modified during pumping.

Recall that the vertical displacements relative to time since the onset of pumping (Fig. 7a) indicated that vertical displacement declined between 35 and 62 days even though pumping had not changed. One-dimensional models could not predict or explain this occurrence. Fig. 13 shows the strain components after 60 days of pumping and indicates that radial extension increases more rapidly than vertical compaction. Thus the observed decrease in vertical compaction can be explained by the fact that the pore space is extending more rapidly in the radial direction than it is compressing in the vertical direction, which means the overall porosity is increasing and allowing more water to enter into storage and therefore causing a decrease in vertical compaction as a function of time.

6. Estimation of horizontal anisotropy from GPS measurements

The previous calculations involved normal strain components that tacitly implied hydraulic and mechanical isotropic behavior. In a hydraulically anisotropic aquifer, the drawdown caused by pumping is directionally dependent on the principle directions of hydraulic conductivity, which implies that the cone of depression would not be radially asymmetric around the pumping well. Several authors have developed techniques to evaluate the hydraulic anisotropy based on observed heads at three or more observation wells (Papadopoulos, 1965; Hantush and Thomas, 1966; Neuman and others, 1984; Masila and Randolph, 1986). In each of these approaches, it is assumed that the anisotropy within the region of interest is constant. At the Mesquite, NV site, the observed heads (Fig. 4) are associated with the pumped well only; therefore, no effects of hydraulic anisotropy would be observed at WX31. However, the measured displacements (Fig. 3) indicate that mechanical anisotropic behavior is occurring—meaning that the principal directions of strain are not aligned with stress field imposed by pumping. Eqs. (5a)–(5d) can be used to calculate the principal directions of strain and the angle of mechanical anisotropy in the horizontal plane.

For the simplified case where only horizontal strain conditions are used, a two-dimensional strain matrix can be defined as

$$\boldsymbol{\varepsilon} = \begin{bmatrix} \varepsilon_{rr} & \varepsilon_{r\theta} \\ \varepsilon_{\theta r} & \varepsilon_{\theta\theta} \end{bmatrix}. \quad (10)$$

The matrix is assumed to be symmetric so that $\varepsilon_{r\theta} = \varepsilon_{\theta r}$. To evaluate the principal values of strain, an eigenvalue problem

$$\boldsymbol{\varepsilon}\mathbf{x} = \lambda\mathbf{x} \quad (11)$$

is solved for the components of ε and rearranging to yield

$$\begin{bmatrix} \varepsilon_{rr} - \lambda & \varepsilon_{r\theta} \\ \varepsilon_{\theta r} & \varepsilon_{\theta\theta} - \lambda \end{bmatrix} \begin{Bmatrix} r \\ \theta \end{Bmatrix} = \begin{Bmatrix} 0 \\ 0 \end{Bmatrix}. \quad (12)$$

Setting the determinant of the matrix in Eq. (12) to zero and rearranging terms yields

$$\lambda^2 - \lambda(\varepsilon_{rr} + \varepsilon_{\theta\theta}) + \varepsilon_{rr}\varepsilon_{\theta\theta} - \varepsilon_{r\theta}^2 = 0, \quad (13)$$

which is a quadratic equation. Because ε is symmetric, two real roots exist and represent the principal values of the strain tensor, which can be expressed as

$$\varepsilon'_{rr} = \frac{\varepsilon_{rr} + \varepsilon_{\theta\theta}}{2} + \sqrt{\left(\frac{\varepsilon_{rr} - \varepsilon_{\theta\theta}}{2}\right)^2 + \varepsilon_{r\theta}^2} \quad (14a)$$

$$\varepsilon'_{\theta\theta} = \frac{\varepsilon_{rr} + \varepsilon_{\theta\theta}}{2} - \sqrt{\left(\frac{\varepsilon_{rr} - \varepsilon_{\theta\theta}}{2}\right)^2 + \varepsilon_{r\theta}^2}. \quad (14b)$$

Expressions from the right-hand-side of Eq. (5a)–(5f) can be substituted into Eq. (14a) and (14b) to yield the principal strains based on the measured displacements. The angle that the principal strains make with the existing east–west, north–south coordinate system is expressed in terms of strains as

$$2\theta = \tan^{-1} \left[\frac{2\varepsilon_{r\theta}}{\varepsilon_{rr} - \varepsilon_{\theta\theta}} \right] \quad (15)$$

where θ represents the local angle of rotation for the system to be in the principal strain directions. That is, it is the angle measured from the endpoints of the displacements shown in Fig. 3. Because these deformations are small relative to the distances involved it is not important from a practical point of view.

Table 4 shows the angles of rotation required for strains to be aligned in the principal directions at each vault pair, measured from $a+r$ (eastward) direction. Note that the system requires more rotation as the distance to the pumping well is shortened. This changing rotation is likely due to the nature of strain in a single anisotropic field rather than a trending anisotropic field within the study area. This will be further investigated in Part 2 of this investigation dealing with numerical simulation of flow and deformation. Fig. 14 shows these rotations along with the magnitude of the principal strain components that can be readily obtained from the values presented in Table 4. Fig. 14 clearly indicates that the angle of rotation is to the northeast with the apparent anisotropy decreasing away from the pumping well. The maximum apparent anisotropy is 3:1 at the pumping well and is nearly isotropic between vaults 10 and 14.

The forces associated with pumping (i.e. hydraulic gradient) are directed toward the pumping well. Therefore, the stress field is aligned radially toward the pumping well also. Consequently, the only mechanism that can cause the observed displacements to diverge

from the radial direction toward the pumping well is an imposed hydraulic anisotropy. Burbey (2001a, b) has shown that greater horizontal deformations occur in coarse-grained deposits even though they typically have a smaller vertical compressibility. It may therefore be concluded that the observed deformation and strain field map (Fig. 14) represent the principal directions of hydraulic conductivity. The use of GPS to characterize the hydraulic conductivity tensor may prove to be a far superior approach than using hydraulic head data because the latter technique assumes that the rotation and the magnitude of the principal directions are constant within the field of observation. The relation between strain and hydraulic conductivity will be further investigated in Part 2, which deals with numerical simulation of flow and deformation.

7. Summary and conclusions

A controlled 62-day aquifer test was conducted in a thick heterogeneous sequence of unconsolidated sedimentary deposits in Mesquite, NV. High precision GPS receivers and antennas were installed at the land surface at different radial distances from the pumped well prior to the test to observe surface deformations prior to and associated with pumping. Highly definable horizontal (radial and tangential) and vertical deformations were recorded during the aquifer test in spite of the fact that a relatively thick, brittle, unsaturated zone of 83 m exists over the pumped aquifer. Precision of the horizontal displacements were 0.2 mm, while the resolution in the vertical direction was determined to be 2 mm. Pumping was cyclic with approximately equal 8 h intervals in between pumping events and with an average daily rate of 9028 m³. Water levels were recorded at the pumping well and at one observation well 1500 m south of the pumped well.

Results indicate that steady-state water-levels were attained after 35–40 days of pumping and the drawdown at the pumped well reached an average level of about 5 m although individual drawdown events (one cycle) regularly reached 10 m. In spite of the small net drawdown recorded, horizontal and vertical deformations reached nearly 10 mm. Vertical subsidence was found to decrease after about 35 days in spite of the fact that the net pumping rate did not change. This decline was found to be the result of a change in the shape of the pore space. Additional storage was accommodated in the horizontal direction as radial extension (pore elongation) increased more rapidly than vertical compression allowing for more water to enter the void space as storage, which manifested in the observance of a noticeable vertical subsidence rebound.

Compressional radial strain was limited to within 200 m of the pumping well, even at the end of the pumping test and is likely the result of cyclic pumping. Near the pumping well the cumulative areal strain is as large as the vertical strain and suggests that horizontal strain is important near the pumping well. In models where horizontal strain is ignored, unrealistically high amounts of subsidence or lower than actual storage would be predicted on the basis of observed water levels near zones of pumping.

Measured displacements show a consistent and definable anisotropic behavior as significant deformation occurs in the tangential direction. These deformations were used to calculate the principal strain directions and the angle of rotation from the existing coordinate system to the principal strain directions. Results indicate that an average rotation of about 20° north of east

occurs. It is concluded that the mechanism responsible for this strain anisotropy is hydraulic anisotropy and that the principal directions of hydraulic conductivity are likely to be aligned with those of the strain directions and magnitudes. This finding indicates that aquifer heterogeneity can be determined without installation of costly monitoring wells, which is significant in these arid zone environments where a thick unsaturated zone typically exists. The results also suggest that steady-state conditions can be predicted without monitoring wells.

Acknowledgment

We would like to thank Michael Johnson of the Virgin Valley Water District for making this aquifer test possible. Mr. Johnson provided access to the site and to logs and pumping data used in this investigation. We also want to express appreciation to Bret Pecoraro for collection of field data during a very hot time of year. Finally, we are grateful to the National Science Foundation for the financial support that made this project possible.

References

- [1] Amelung, F., D, L., Galloway, J.W., Bell, H.A., Zebker, H.A., Laczniak, R.J., 1999. Sensing ups and downs of Las Vegas: InSAR reveals structural control of land subsidence and aquifer system deformation. *Geology* 27, 483–486.
- [2] Bell, J.W., 1981. Subsidence in Las Vegas Valley. Nevada Bureau of Mines and Geology Bulletin 95, 81.
- [3] Bell J.W. and Price, J.G., 1991. Subsidence in Las Vegas Valley, 1980–91. Nevada Bureau of Mines and Geology Open-File Report 93-5, p. 182.
- [4] Bell, J.W., Amelung, F., Ramielli, A.R., Blewitt, G., 2002. Land subsidence in Las Vegas, Nevada, 1935–2000: new geodetic data show evolution, revised spatial patterns and reduced rates. *Environmental & Engineering Geoscience* 8, 155–174.
- [5] Biot, M.A., 1941. General theory of three-dimensional consolidation. *Journal of Applied Physics* 12, 155–164.
- [6] Biot, M.A., 1955. Theory of elasticity and consolidation for a porous anisotropic solid. *Journal of Applied Physics* 26, 182– 185.
- [7] Blewitt, G., 1993. Advances in Global Positioning System technology for geodynamics investigations, in *Contributions of Space Geodesy to Geodynamics: Technology*, Ed. by D.E. Smith and D.L. Turcotte, p. 195-213, Pub. by American Geophysical Union (Geodynamics Series Vol. 25), Washington DC, ISBN 0-87590-526-9.
- [8] Blewitt, G., 1997. Basics of GPS Technique: Observation Equations. *Geodetic Applications of GPS. Lecture Notes for Nordic Autumn School, Nordic Geodetic Commission, Bastad, Sweden, 26-31 August 1996*, ed. Bo Jonsson.
- [9] Blewitt, G., 1998. GPS data processing methodology: from theory to applications. In: Teunissen, P.J.G., Kleusberg, A. (Eds.), *GPS for Geodesy*. Springer-Verlag, Berlin, ISBN: 3-540-63661-7, pp. 231–270.
- [10] Burbey, T.J., 1999. Effects of horizontal strain in estimating specific storage and compaction in confined and leaky aquifer systems. *Hydrogeology Journal* 7, 521–532.
- [11] Burbey, T.J., 2001a. Stress–strain analyses for aquifer-system characterization. *Groundwater* 39, 128–136.
- [12] Burbey, T.J., 2001b. Storage coefficient revisited: is purely vertical strain a good assumption? *Groundwater* 39, 458–464.
- [13] Burbey, T.J., 2002, The influence of faults in basin-fill deposits on land subsidence, Las Vegas Valley, Nevada, USA: *Hydrogeology Journal*, v. 10, p. 525–538.
- [14] Burbey, T.J., 2003. Use of time-subsidence data during pumping to characterize specific storage and hydraulic conductivity of semi-confining units. *Journal of Hydrology* 281, 3–22.
- [15] Burbey, T.J., Helm, D.C., 1999. Modeling three-dimensional deformation in response to pumping of unconsolidated aquifers. *Environmental & Engineering Geoscience* 5, 199–212.
- [16] Dixon, G.L., and Katzer, T., 2002. Geology and hydrology of the Lower Virgin River Valley in Nevada, Arizona, and Utah. Technical report VVWD-41, p. 126.
- [17] Fetter, C.W., 1994. *Applied Hydrogeology*, 3rd Edition Prentice Hall, New Jersey, NJ p.

691.

- [18] Galloway, D.L., Hednut, K.W., Ingebritsen, S.E., Phillips, S.P., Peltzer, G., Rogez, F., P, A., 1998. Rosen, InSAR detection of system compaction and land subsidence, Antelope Valley, Mohave Desert, California. *Water Resources Research* 34, 2573–2585.
- [19] Hanson, R.T., 1989. Aquifer-system compaction, Tucson Basin and Avra Valley, Arizona. US Geological Survey Water-Resources Investigations Report 88-4172, p. 69
- [20] Hanush, M.S., Thomas, R.G., 1966. A method for analyzing a drawdown test in anisotropic aquifers. *Water Resources Research* 2, 281–285.
- [21] Hein, G.W., Riedl, B., 1995. In: Barends, Brouwer, Schroder (Eds.), *A High-Precision Real time Land Subsidence Monitoring System Based on DGPS Land Subsidence*. Balkema, Rotterdam, pp. 159–167.
- [22] Helm, D.C., 1994a. Hydraulic forces that play a role in generating fissures at depth. *Bulletin of the Association of Engineering Geologists* 31, 293–302.
- [23] Helm, D.C., 1994b. Horizontal movement in a Theis-Theim confined system. *Water Resources Research* 30, 953–964.
- [24] Helm, D.C., 1987. Three-dimensional consolidation theory in terms of the velocity of solids: *Geotechnique*, v. 37, p. 369–392.
- [25] Heywood, C.E., Galloway, D.L., and Stork, S.V., 2002. Ground Displacements Caused by Aquifer-System Water-level Variations Observed Using Interferometric Synthetic Aperture Radar Near Albuquerque, New Mexico. US Geological Survey Water Resources Investigations Report 02-4235, p. 18.
- [26] Hoffmann, J., Zebker, H.A., Galloway, D.L., Amelung, F., 2001. Seasonal subsidence and rebound in Las Vegas Valley, Nevada, observed by synthetic aperture radar interferometry. *Water Resources Research* 37, 1551–1566.
- [27] Ikehara, M.E., 1994. Global Positioning System surveying to monitor land subsidence in Sacramento Valley, CA, USA. *Hydrological Sciences Journal* 39, 417–429.
- [28] Ikehara, M.E., S.P. Phillips. 1994. Determination of land subsidence related to ground-water-level declines using global positioning system and leveling surveys in Antelope Valley, Los Angeles and Kern Counties, California, US Geological Survey Water-Resources Investigations Report, 94-4184.
- [29] Ikehara, M.E., S.K. Predmore, and D.J. Swope, 1997, Geodetic network to evaluate historical elevation changes and to monitor land subsidence in lower Coachella Valley, California, 1996: U.S. Geological Survey Water-Resources Investigations Report 97-4237, 1 map.
- [30] Johnson, M., Dixon, G., Rowley, P.D., Katzer, T.C., Winters, M., 2002. Hydrology and Groundwater Conditions of the Tertiary Muddy Creek Formation in the lower Virgin River Basin of Southeastern Nevada and Adjacent Arizona and Utah. Geological Society of American 2002 Rocky Mountain Section Annual Meeting. Cedar City, UT, May 10, 2002, pp. 284–315.
- [31] Langenheim, V.E., Glen, J.M., Jachens, R.C., Dixon, G.L., Katzer, T.C., R.L. Morin, 2000. Geophysical Constraints on the Virgin River Depression, Nevada, Utah, and Arizona. US Geological Survey Open File Report 00-407, p. 12.
- [32] Leake, S.A., Prudic, D.E., 1991. Documentation of a computer program to simulate

- aquifer-system compaction using the modular finite difference model ground water flow model. Techniques of Water Resources Investigations of the United States Geological Survey, Chapter A2, Book 6, p. 74.
- [33] Masila, M.L., Randolph, R.B., 1986. Methods and computer program documentation for determining anisotropic transmissivity tensor components of two-dimensional ground- water flow. US Geological Survey Open-File Report 86-227, p. 64.
- [34] Neuman, S.P., Walter, G.R., Bentley, H.W., Ward, J.J., Gonzalez, D.D., 1984. Determination of horizontal aquifer anisotropy with three wells. *Ground Water* 22, 66–72.
- [35] Papadopoulos, I.S., 1965. Nonsteady flow to a well in an infinite anisotropic aquifer, Proceedings of the Dubrovnik Symposium on the Hydrology of Fractured Rocks, International Association of Scientific Hydrology 1965 pp. 21–31.
- [36] Pope, J.P., Burbey, T.J., 2004. Multiple-aquifer characterization from single borehole extensometer records. *Ground Water* 42, 45–58.
- [37] Riley, F.S., 1969. Analysis of borehole extensometer data from central California. In: Tison, L.J. (Ed.), *Land Subsidence*, Vol. 2. Tokyo International Association of Scientific Hydrology Publication 89, Merbien, pp. 423–431.
- [38] Riley, F.S., 1984. Land subsidence. In: Johnson, A.I., Carbognin, L., Ubertini, L. (Eds.), *Proceedings of the 3rd International Symposium on Land Subsidence*, Venice, Vol. 151. IAHS Publications, Wallingford, pp. 169–186.
- [39] Shumann, H.H., and Anderson, S.R., 1988. Land-subsidence measurements and aquifer-compaction monitoring in Tucson Basin and Avra Valley, Arizona. US Geological Survey Water-Resources Investigations Report 88-4167, p. 15.
- [40] Smith, I.M., Griffiths, D.V., Hsieh, P.A., Burbey, T.J., 1996. BIOT4 (version 4.0). A Finite-element model to simulate axisymmetric/plane-strain solid deformation and fluid flow in a linearly elastic porous media. User Documentation, p. 54.
- [41] Smith, I.M., Griffiths, D.V., 1988. *Programming the finite element method*, seconded. John Wiley and Sons, Chinchester.
- [42] Sneed, M., 2001. Hydraulic and mechanical properties affecting ground-water flow and aquifer-system compaction, San Joaquin Valley, California. United States Geological Survey Open File Report 01-35, p. 26.
- [43] Sneed, M., Ikehara, M.E., Galloway, D.L, Amelung, F., 2001. Detection and measurement of land subsidence using global positioning system and interferometric synthetic aperture radar, Coachella Valley, California, 1996–98. US Geological Survey Water-Resources Investigations Report 01- 4193, p. 26.
- [44] Wilson, A.M., Gorelick, S., 1996. The effects of pulsed pumping on land subsidence in the Santa Clara Valley, California. *Journal of Hydrology* 174, 375–396.
- [45] Yerkes, R.F., Castle, R.O., 1969. Surface deformation associated with oil and gas field operation in the United States. In: Tison, L.J. (Ed.), *Land Subsidence* 1, Vol. 88. 1st International Association of Scientific Hydrology Publication, Wallingford, pp. 55-64.

List of Tables

- Table. 1 Monthly production of Water District wells: April-September, 2003
- Table. 2 Three phases of GPS campaign to monitor land deformation
- Table. 3 Calculated transmissivity (T) and storage coefficient (S) values based on time-drawdown data at WX31
- Table. 4 Magnitudes of the principal directions of strain associated with each pair of vaults and the local rotation angle that the strain matrix must be rotated to be in the principal direction

List of Figures

- Figure. 1 Location of study area showing well and vault locations (circles) and inferred regional potentiometric surface (dashed lines) given in meters AMSL.
- Figure. 2 Pumping well (WL31) design and associated lithologic log.
- Figure. 3 Plan view of field site showing the magnitude of horizontal deformation after 22 days of pumping.
- Figure. 4 Well WL31 hydrograph resulting from cyclic pumping for the 62-day aquifer test.
- Figure. 5 Well WL31 hydrograph resulting from cyclic pumping of well WL31 for the 62-day aquifer test.
- Figure. 6 Radial displacement vs. (a) time and (b) distance for selected vault locations resulting from pumping WX31. Accuracy of plotted values is ± 0.2 mm
- Figure. 7 Vertical displacement vs. (a) time and (b) distance for selected vault locations resulting from pumping WX31. Accuracy of plotted values is ± 5 mm
- Figure. 8 Radial strain as a function of time for selected vault locations.
- Figure. 9 Tangential or hoop strain as a function of time for selected vault locations.
- Figure. 10 Relation of areal strain (hoop+radial) to vertical strain as a function of distance from the pumping well. Volume strain is the sum of areal and vertical strains
- Figure. 11 Vertical strain as a function of time for selected vault locations.
- Figure. 12 Normal strain components as a function of distance from the pumping well after 20 days since the start of pumping.
- Figure. 13 Normal strain components as a function of distance from the pumping well after 60 days since the start of pumping.
- Figure. 14 Strain ellipses centered on point of measurement. Rotation angle represents rotation to the principal strain directions. Shape of ellipse shows relative degree of anisotropy in horizontal direction at each location. Data are from Table 4.

Well	Dist.(m) and Direction relative to WX31	Monthly Production 2003 in Cubic Meters					
		April	May	June	July	August	September
27	4000 NNW	108,497	52,805	166,051	193,928	166,495	101,651
28	6000 NW	104,377	42,653	0	0	0	0
30	5600 S	123,915	27,642	0	0	0	0
31	–	0.00	32,822	267,344	280,617	283,762	267,912
33	9200 N	0.00	165,496	267,505	319,262	322,567	313,279

Table 1

Phase	Duration	Instrumentation
Pre-production	-7 to -1 days	10 stations
Initial Production	0-22 days	10 stations
Continued Production	23-62 days	5 stations (VT 3, 6, 10, 14, WL VX)

Table 2

Method	T (m ² /d)	K (m/d)	S	S _s (1/m)
Theis (short)	1280	5.4	0.00117	4.9×10^{-6}
Theis (long)	720	3.0	0.067	2.8×10^{-4}
Hantush (long)	450	–	–	–
Cooper-Jacob (top)	1400	–	0.0014	–
Cooper-Jacob (bottom)	680	–	0.107	–
Burbey	720	3.0	–	2.8×10^{-6}
Katzer & Dixon	1850	–	–	–

‘Short’ refers to an individual 8-h pumping cycle and ‘long’ refers to average daily drawdown over 22 days. Katzer & Dixon value is from Katzer and Dixon (2002); Burbey value is based on method of Burbey (2003).

Table 3

Vaults	θ_p	ε'_{rr}	$\varepsilon'_{\theta\theta}$
VT01-02	22.2	4.484×10^{-6}	-3.268×10^{-5}
VT02-03	19.4	3.674×10^{-6}	-1.984×10^{-5}
VT03-04	14.5	6.077×10^{-6}	-1.199×10^{-5}
VT04-06	12.7	8.047×10^{-6}	-8.764×10^{-6}
VT06-10	11.3	6.175×10^{-6}	-6.686×10^{-6}

These results are graphically represented in Fig. 14.

Table 4

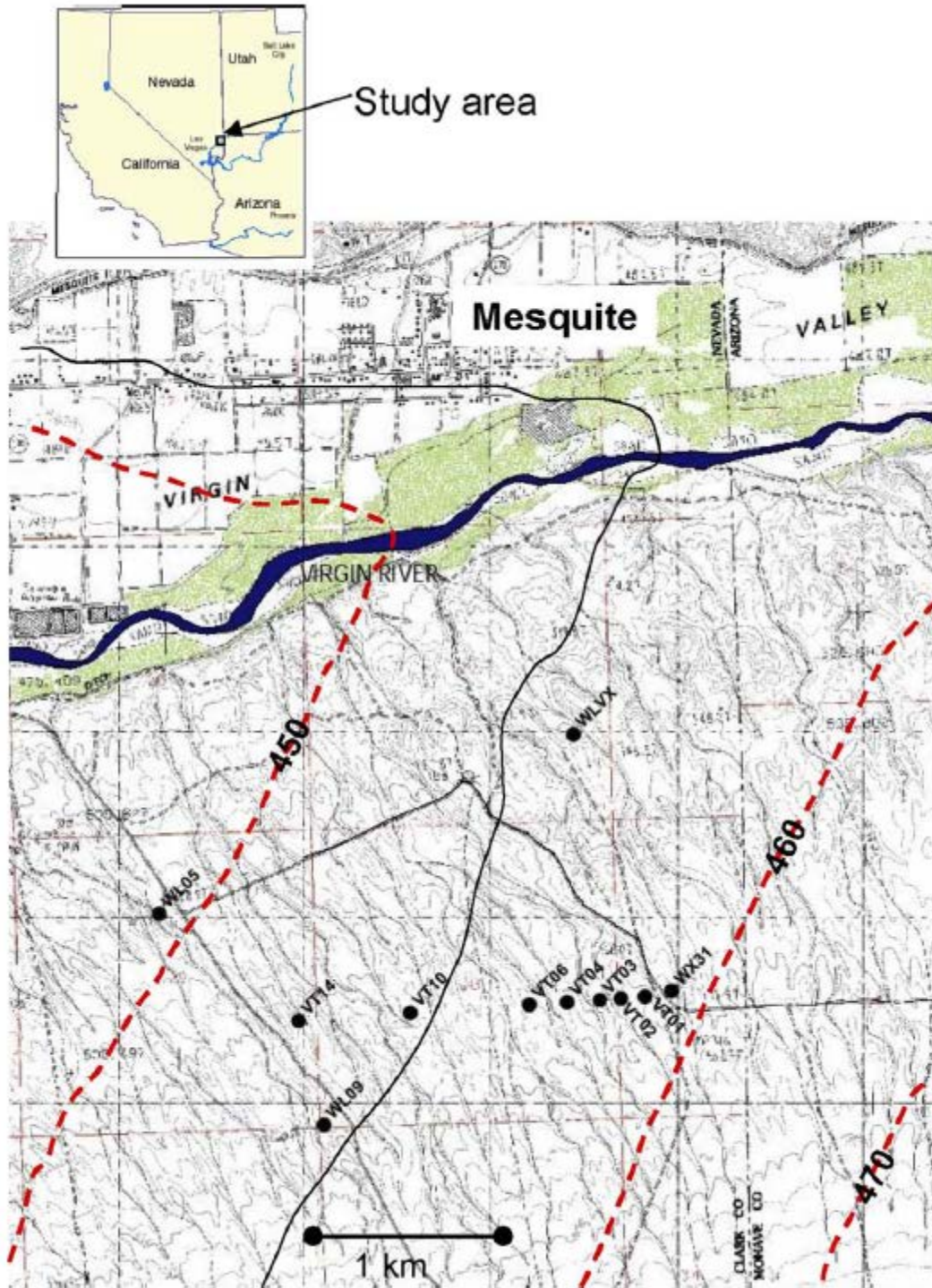


Figure 1

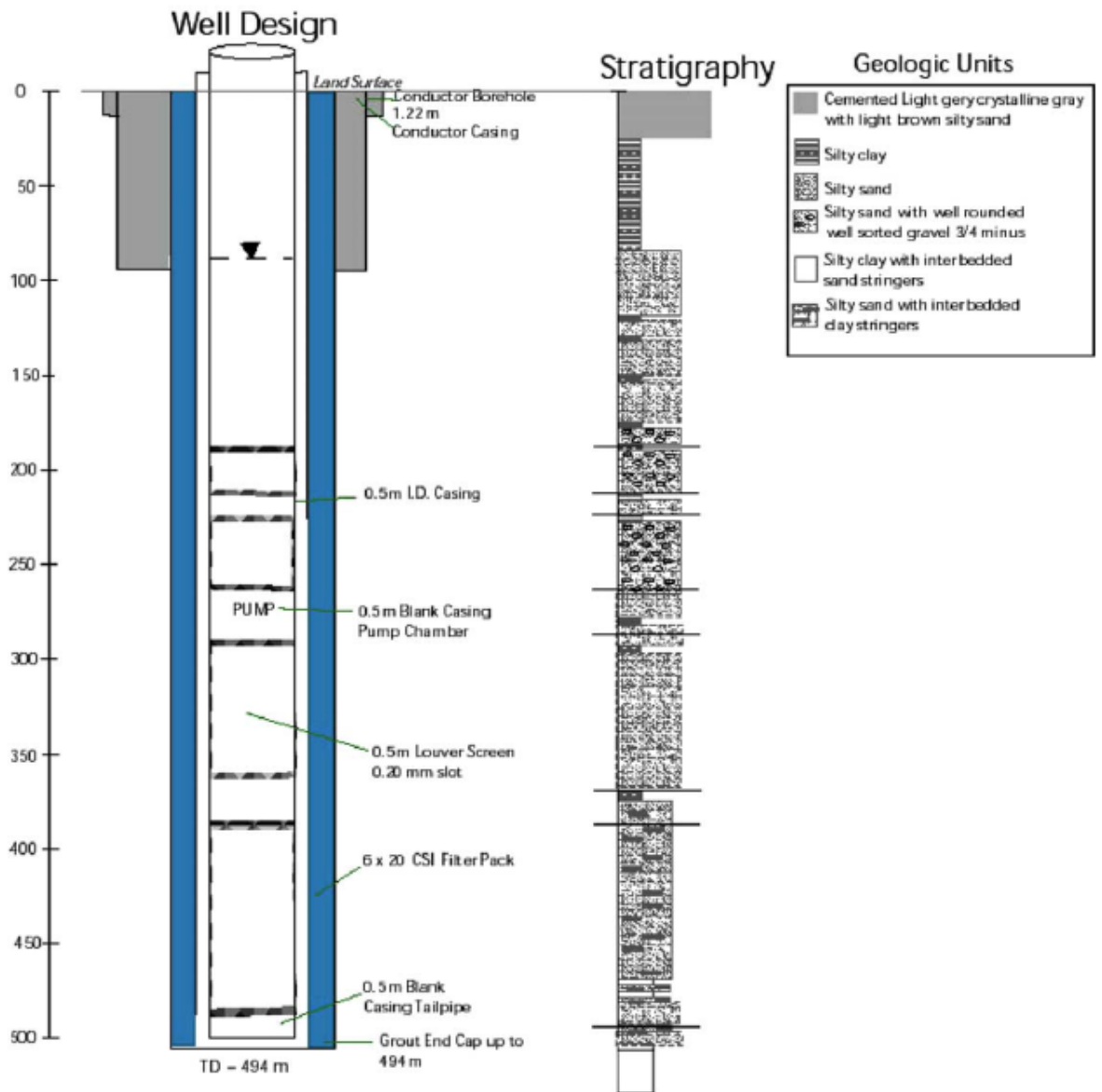


Figure 2

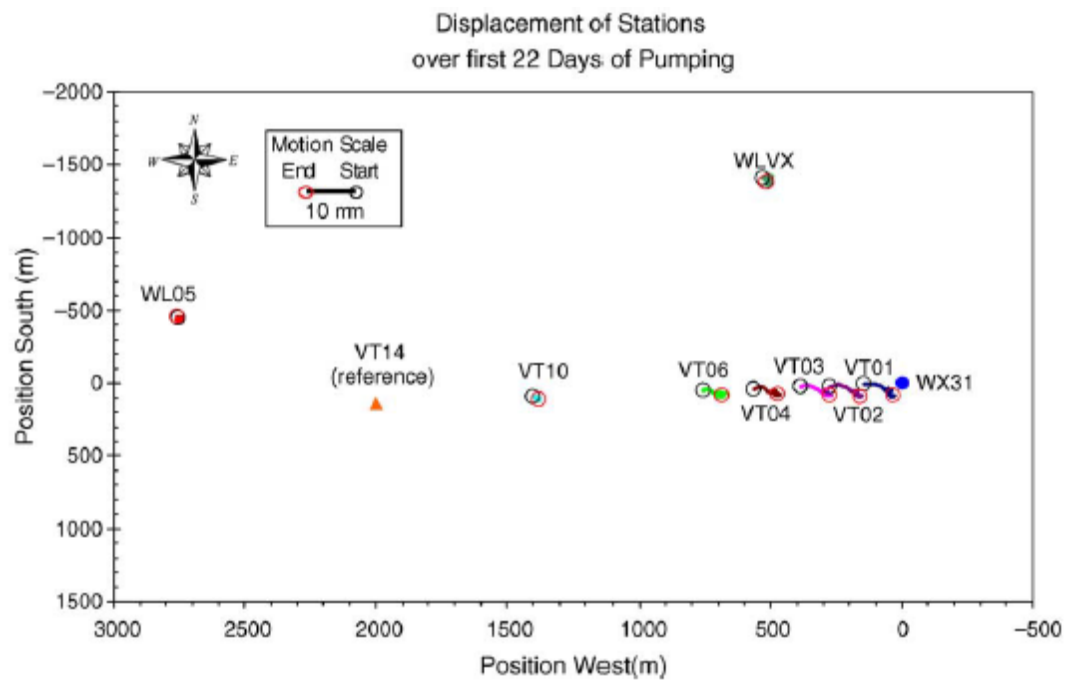


Figure 3

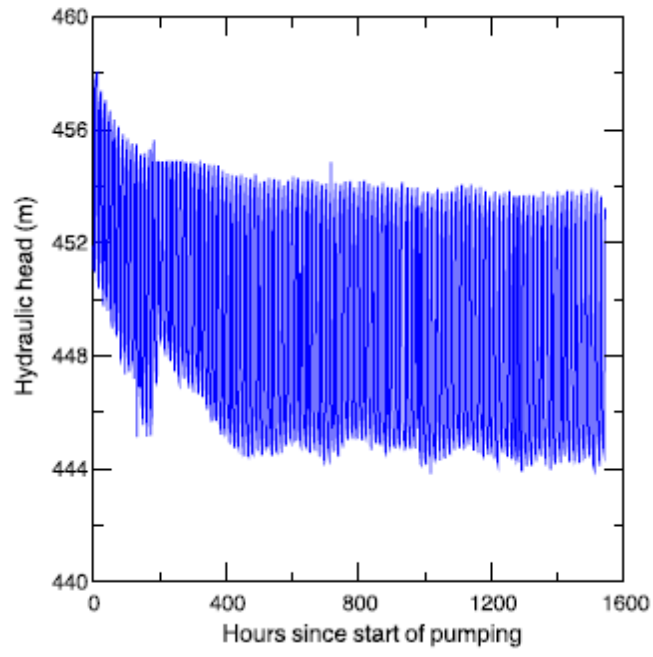


Figure 4

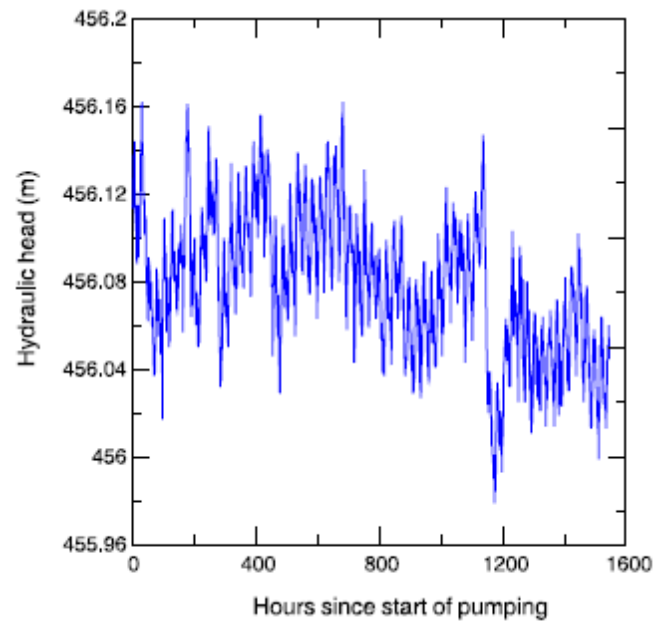


Figure 5

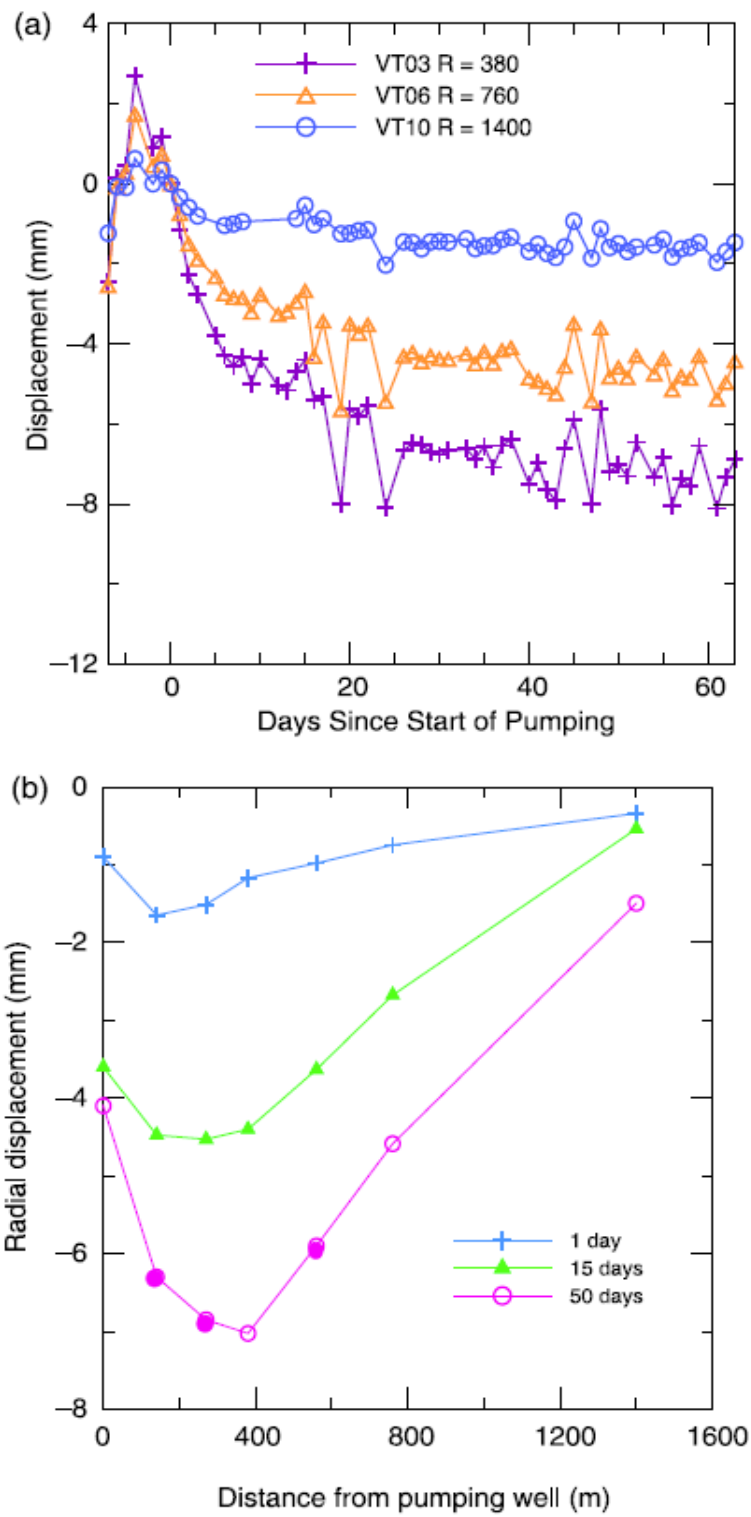


Figure 6

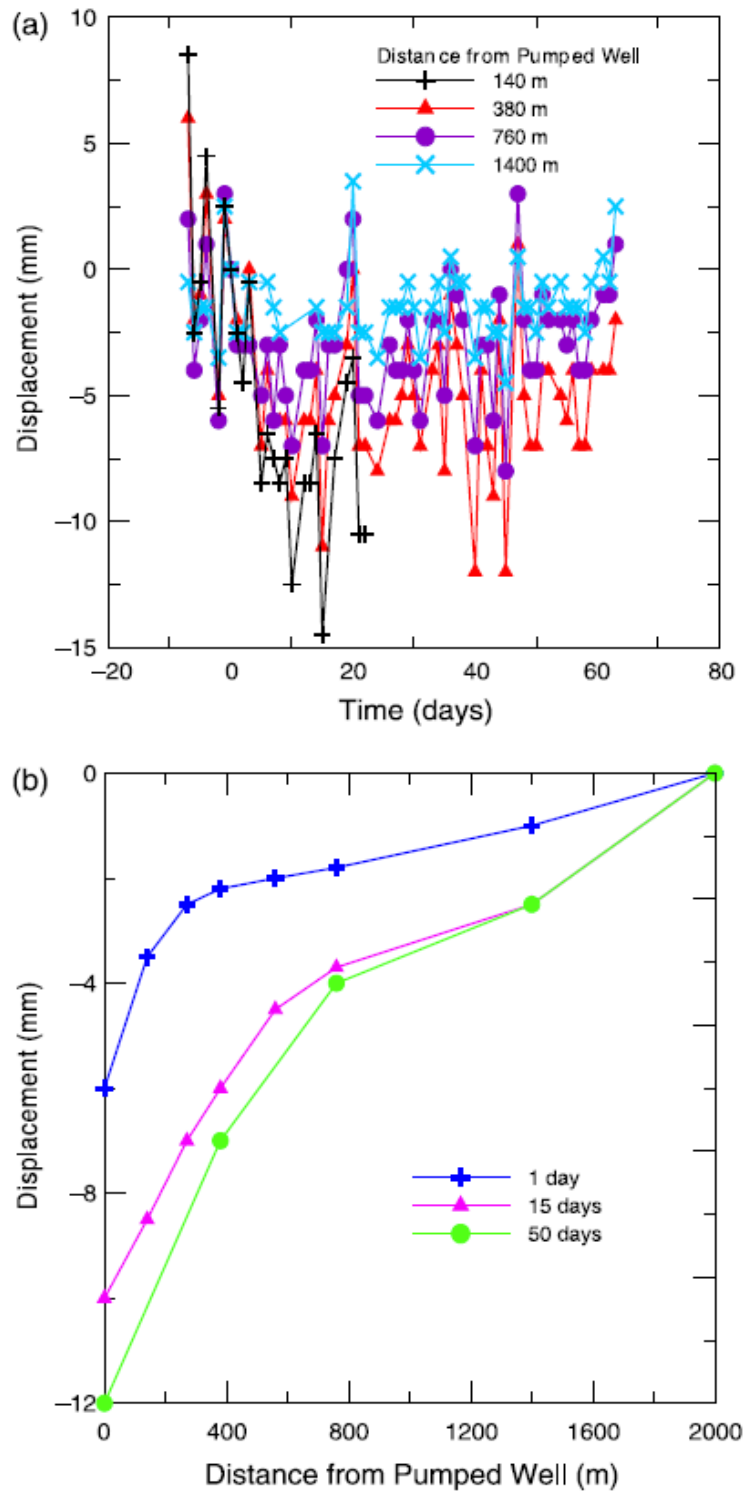


Figure 7

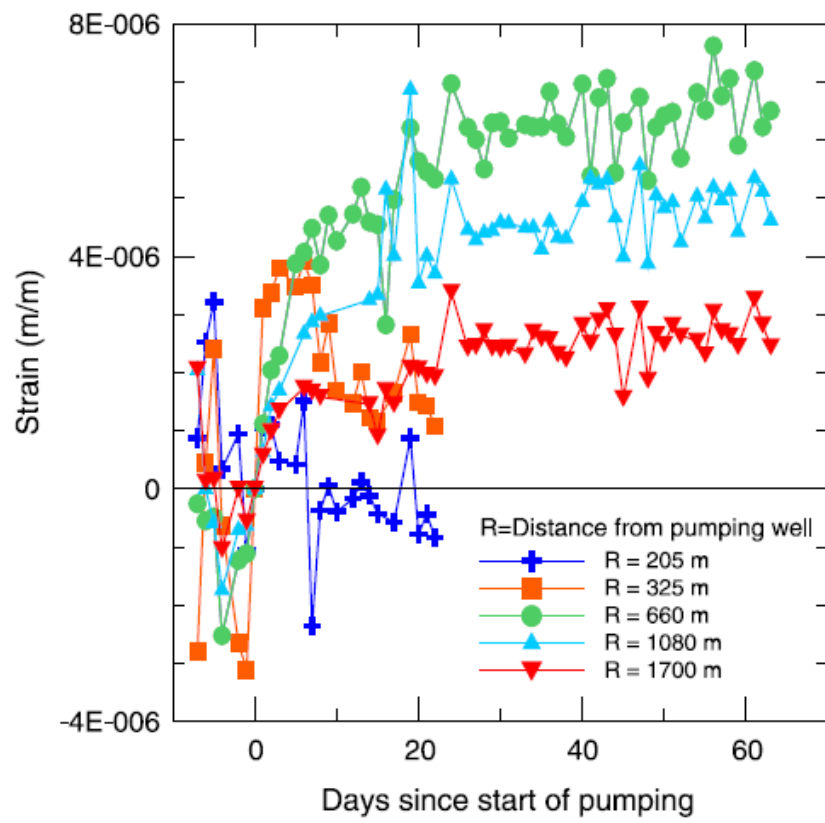


Figure 8

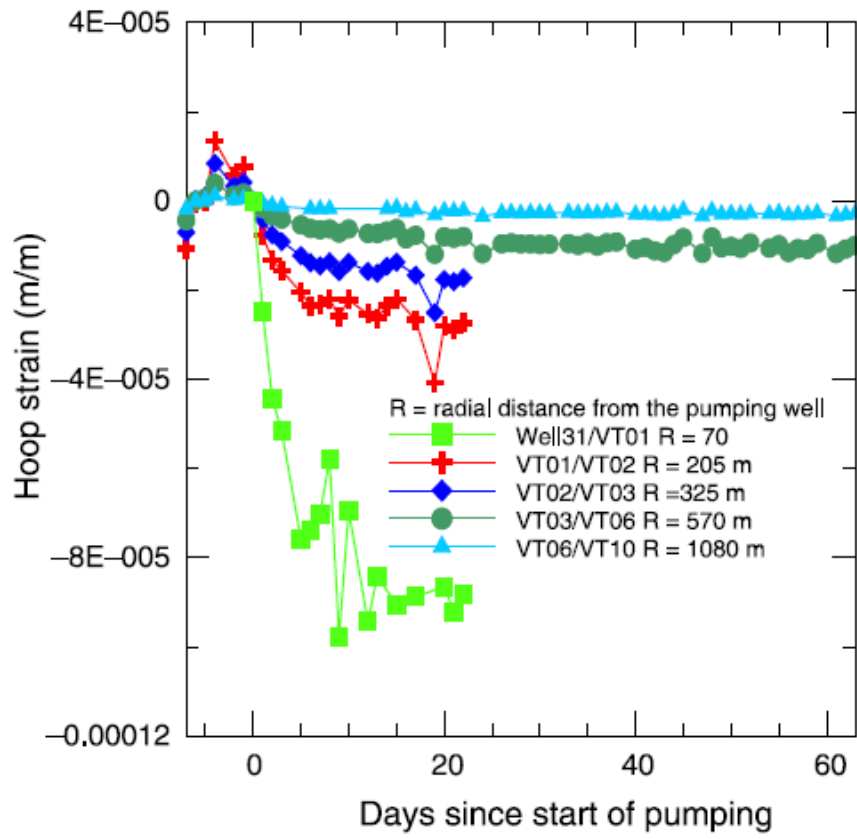


Figure 9

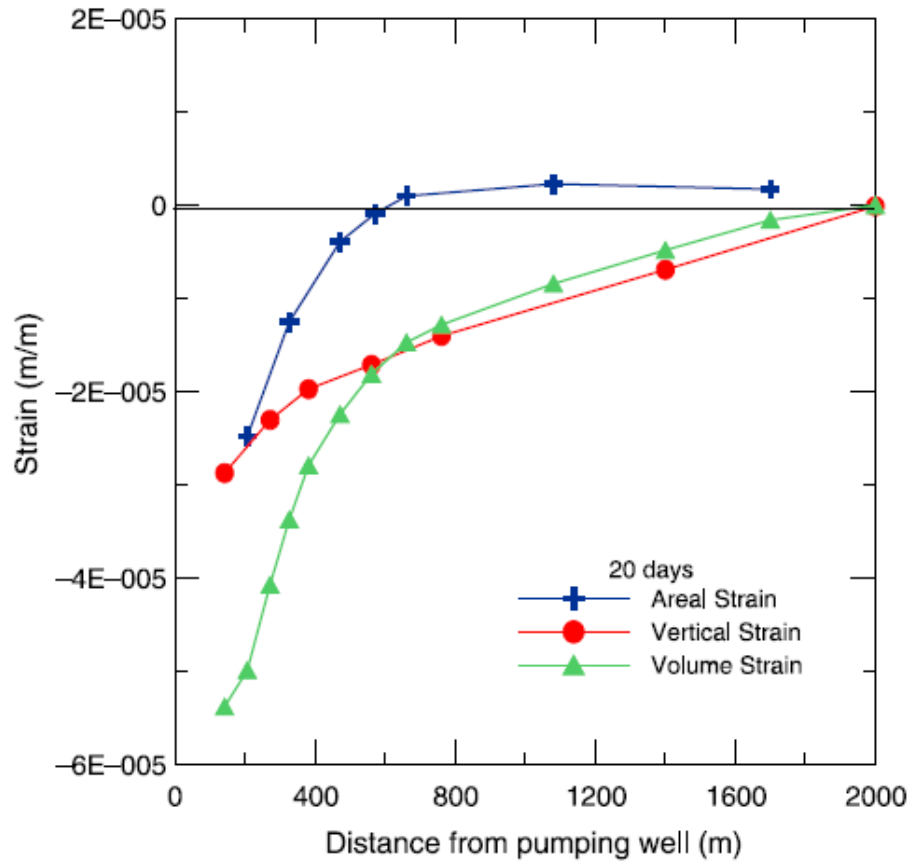


Figure 10

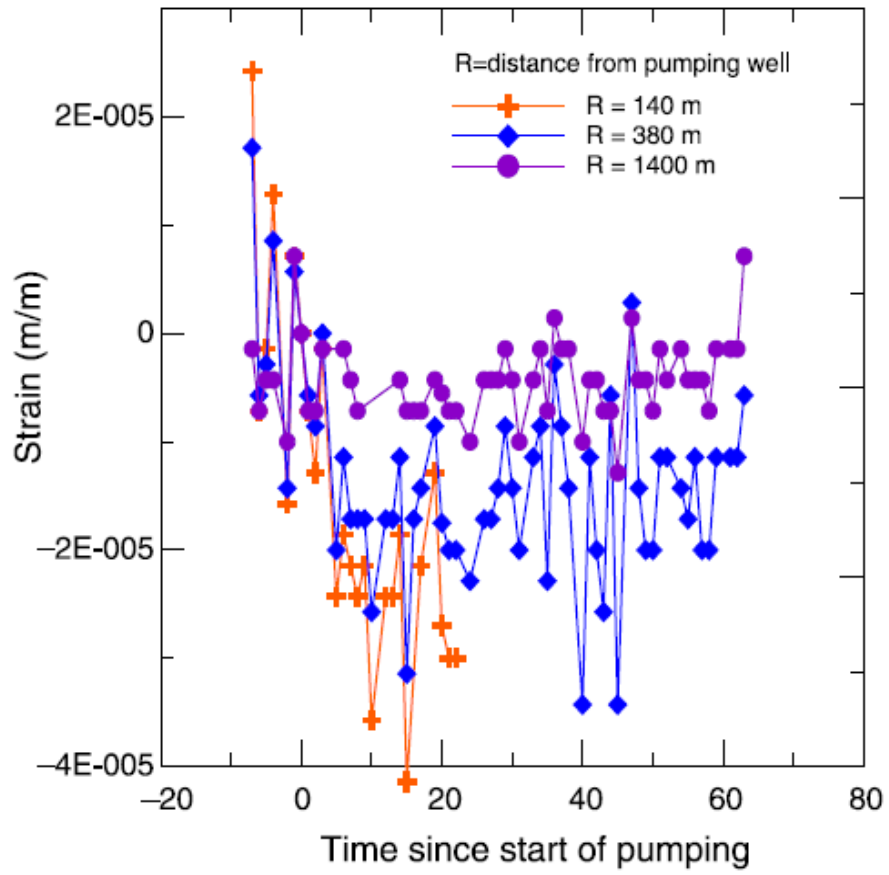


Figure 11

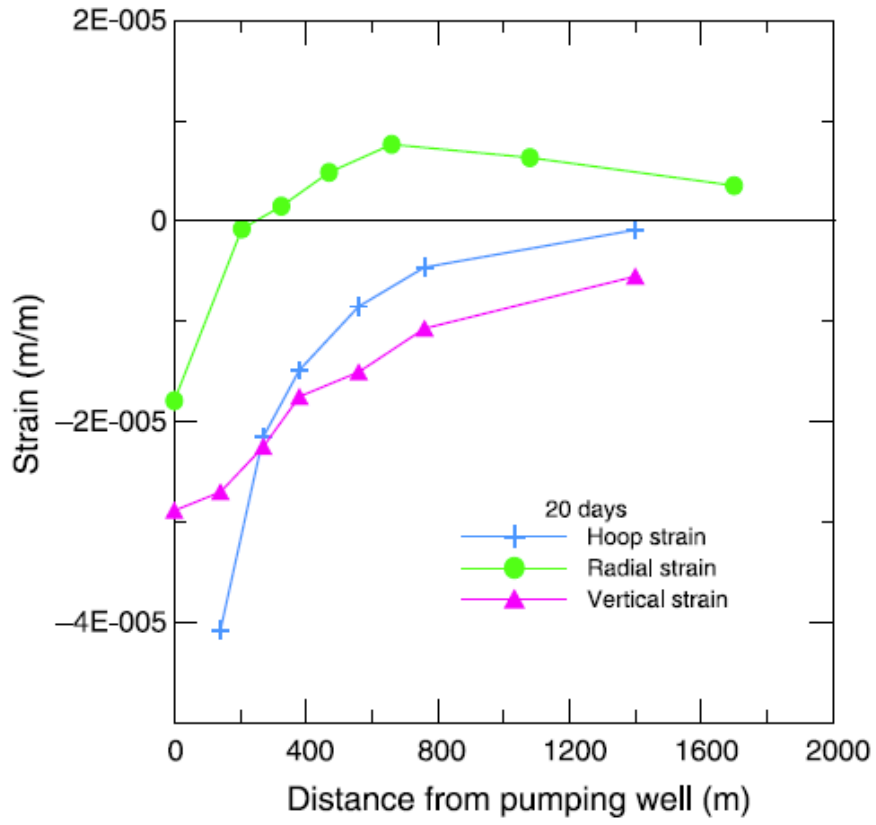


Figure 12

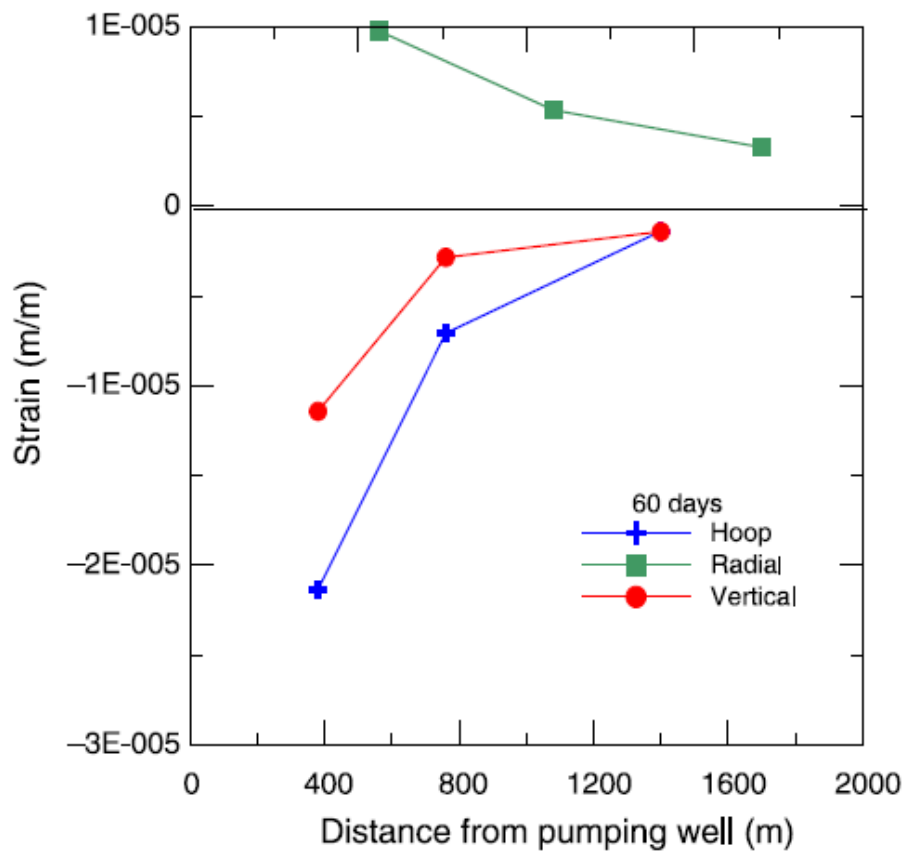


Figure 13

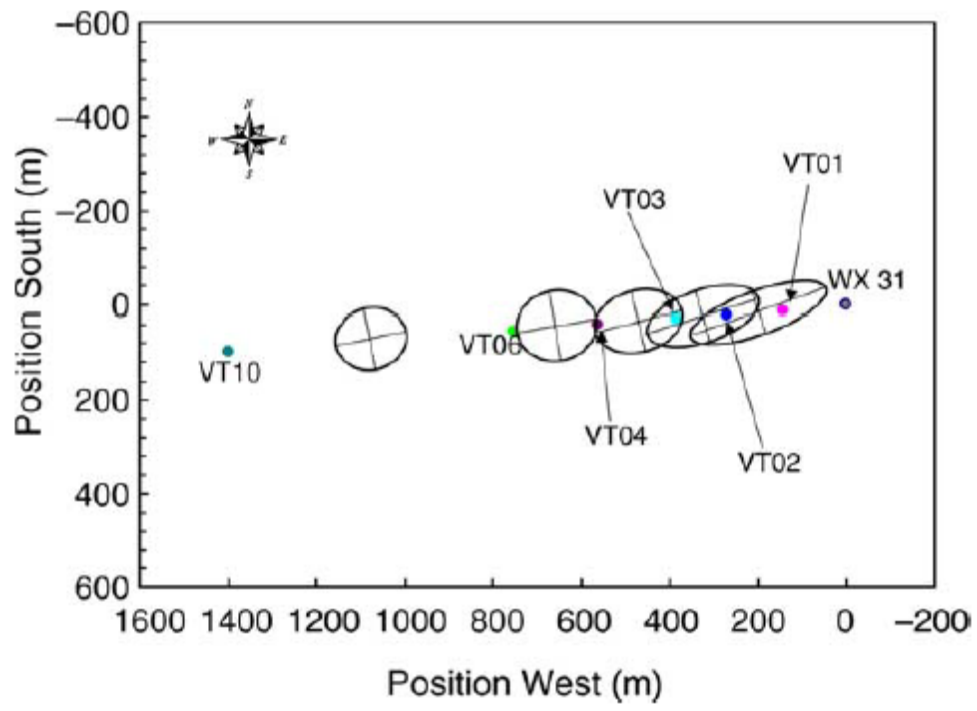


Figure 14